Textile Research Journal

Original research article

Textile Research Journal
1–18

DOI: 10.1177/00405175261468519
journals.sagepub.com/home/trj
Sage

Computational models for predicting air permeability and thermal properties of polyester textile structures

Aušra Gadeikytė[1,2], Mindaugas Kurmis[2], Darius Drungilas[2] and Rimantas Barauskas[1]

Abstract

This study develops pore-scale computational models to predict air permeability and thermal properties of one-layer, two-layer, and three-dimensional polyester textile structures. Accurate prediction of airflow and heat transfer in multilayer textile structures is essential for evaluating the thermal insulation and ventilation characteristics of protective clothing while ensuring thermal comfort. Compared with previous studies, the proposed pore-scale models examine the combined effects of multilayer textile structure and additional ventilation on airflow and heat transfer. The models were created in COMSOL Multiphysics 6.2 using Navier-Stokes and Brinkman equations for airflow and the energy equation for heat transfer simulations in the laminar flow regime. The results showed that when the complexity of textile structures increased from one-layer to three-dimensional structures, the air permeability decreased from 1257.1 mm/s to approximately 447.9 mm/s, and the thermal resistance increased from 0.0144 to 0.123 m^2 K/W. Additional ventilation improved heat extraction, achieving an effective heat transfer coefficient of 53.64 W/m^2 K at a flow rate of 0.5 dm^3/min and an inlet air temperature of 10°C. The numerical predictions showed good agreement with experimental data reported in the literature, confirming the applicability of the developed models for the analysis of airflow and thermal characteristics of multilayer textile structures.

Keywords

3D textile, additional ventilation, thermal comfort properties, air permeability

In recent years, computational methods, including the finite element method, have been widely used as a sustainable approach to analyze heat and moisture transfer through textile structures. In prior applications, computational models have gained significance because such simulations provide an efficient and cost-effective method for analyzing heat and moisture transfer.[1–3] For instance, the applied design and computational model may precisely estimate heat transfer through multilayer textiles with complex geometry, saving raw materials, energy, labor costs, and time during clothing production.[4] Such methods are increasingly used to assess physiological responses and thermal comfort under a variety of conditions, offering an efficient alternative to human testing.[5,6] Moreover, computational simulations allow a realistic representation of physical processes that occur between human skin and textiles. However, the development of such numerical modeling tools and methods is a complex task because it requires taking into account factors such as the clothing microclimate, airflow, heat and moisture transfer, and human thermophysiological responses.[5] According to ISO

[1]Department of Applied Informatics, Kaunas University of Technology, Kaunas, Lithuania
[2]Klaipeda University, Klaipeda, Lithuania

Corresponding author:
Aušra Gadeikytė, Department of Applied Informatics, Kaunas University of Technology, Studentu Str. 50-403a, Kaunas, LT-51368, Lithuania.
Email: ausra.gadeikyte@ktu.lt

11092,[7] thermal comfort is determined by its physical properties, which include a complex interaction of heat and mass transfer. These processes may occur independently or concurrently. They are time-dependent and can be studied in either steady-state or transient conditions.[7]

One of the challenges for textile designers is to ensure thermal comfort. Thermophysiological comfort refers to the exchange of heat and moisture between the skin and the open air, which maintains a comfortable body temperature in the range of approximately 36.5–37.5°C.[8] Environmental factors have a significant impact on thermal comfort, as certain environments require specific textiles and material compositions. For example, textile materials with high thermal insulation are recommended for cold and dry environments. In cold, rainy (humid), and windy conditions, it is more effective to use insulated textile materials combined with a water vapor permeable membrane, which protects against wind chill and precipitation while allowing internal moisture to evaporate, thus maintaining thermal comfort.[9] It is well known that air permeability (AP) and thermal resistance are identified as the essential thermal comfort properties of textiles.[9,10] AP is related to the ability of air to pass through a material, which is essential for maintaining breathability and preventing overheating.[11] The AP of a fabric depends on its air porosity, which ultimately affects its openness. Thermal resistance refers to the thermal insulation characteristics of a textile material. Increased thermal resistance results in lower heat loss.[12]

These important properties have been investigated in various studies using experimental and computational methods. Shen et al.[13] proposed a computational fluid dynamics model to simulate the hygroscopic heating efficiency and heat transfer properties of textiles. The hygroscopic and exothermic regions of the textile were modeled as symmetrical configurations. It was found that higher ambient temperatures led to a more pronounced warming effect.[13] Wang et al.[14] numerically investigated the heat and moisture transfer properties of plain weave fabric models in the horizontal and vertical directions. The study also explored how weave structure and fabric cover impact fabric heat flux and water vapor concentration.[14] Ali et al.[15] provided a one-unit-cell computational model to predict the AP and thermal conductivity of interlock and rib-knitted fabrics. It was demonstrated that extending the stitch length increases AP and reduces effective thermal conductivity.[15] Miśkiewicz et al.[16] performed a numerical simulation of heat flow through a composite material developed on the basis of basalt fabric. The model was based on simplified geometric and isotropic assumptions that could not completely incorporate the complex fiber structure.[16]

Furthermore, recent research has increasingly focused on the role of ventilation and airflow in clothing systems. In windy conditions or when walking, ventilation allows air to move through textiles or the microclimate air layer between the skin and the fabric. Therefore, increased air movement inside the clothing system affects its insulation properties. In such scenarios, to more accurately assess the thermal insulation properties of clothing, dynamic thermal resistance should be taken into account.[17–19] In most cases, ventilation flow is caused by the movement of fabric layers when the wearer moves, but it can also be specifically created using specialized ventilators or other devices.[20] Several studies have investigated how forced ventilation affects clothing systems. Sun and Jasper [21] introduced a lightweight wearable convective cooling system in which a series of microfans was integrated into a ribbon attached to a garment to enhance cooling through both convective and evaporative heat transfer. A simplified 2D mathematical model, which included microfans and a textile undergarment, was numerically simulated at four different inlet air velocity settings.[21] You et al.[22] investigated the average temperature changes of human skin and the microenvironment under the influence of mine ventilation clothing (cooling suits) made of different clothing materials using a macroscale model of a human torso wearing the mine ventilation clothing. However, the model assumed ideal conditions and did not take into account the influence of the surrounding environment.[22] Yichen et al.[23] created a three-dimensional (3D) transient model of a cylindrical air layer–porous textile–external environment system to represent a human torso shape. The researchers examined the impact of environmental factors, such as wind velocity, temperature, humidity, and air layer thickness, on heat and moisture transfer. The simulation results demonstrated that as wind velocity increases, convective heat transfer dominates during dry heat transfer.[23] Recent numerical studies have indicated that the arrangement, porosity, thickness, and permeability distribution of multilayer textile systems have a significant impact on heat transfer and thermal insulation behavior. Improved insulation properties are generally achieved when more porous layers are positioned closer to the skin, while less permeable layers act as an external barrier, reducing internal airflow and convective heat loss in windy conditions.[19,24] According to Codau et al.,[25] most modeling approaches for heat and mass transfer through textile materials are at the macroscopic level, with microscopic details removed in order to reduce numerical and physical complexity. Furthermore, recent computational fluid dynamics (CFD) studies have demonstrated that realistic microclimate geometry, airflow direction, and local textile permeability affect thermal resistance in porous textile systems.[26]

Table 1. Measured construction parameters and evaluated AP of the sample.[27]

Sample	Set density warp/weft	Thickness (mm)	Measured AP (mm/s)	Coefficient of variation (%)
Plain weave	29.3/15	0.468	1268.33	1.42

Recent computational modeling studies have highlighted the complex interactions between heat, moisture, and textile structure, especially at the interface between skin, clothing, and the environment, where these exchanges directly influence thermal comfort. Despite these advances, existing computational models still have several limitations. Most studies are based on simplified geometrical representations and focus primarily on one-layer textile structures, with only limited attention given to extending these models to more complex multilayer and 3D configurations.[19] Furthermore, the combined effects of multilayered textile structures and forced airflow within the clothing microclimate have not been sufficiently investigated, particularly within integrated pore-scale modeling approaches.[19,23] Pore-scale models enable a more detailed representation of airflow and heat transfer processes through textile structures. In such models, the effects of microstructural features can be characterized using the effective properties of porous media, such as local permeability and porosity.

To address these limitations, the aim of this study is to develop and validate pore-scale computational models for predicting the AP and thermal characteristics of one-layer, two-layer, and 3D polyester textile structures. In contrast with previous studies, the developed computational models combine multilayer textile structures and additional ventilation, taking into account local permeability and porosity effects. Compared with simplified macroscale models, the developed models provide a more detailed representation of airflow and heat transfer within porous textile structures. The models also allow controlled investigation of ventilation parameters and multilayer textile structures that are difficult to characterize experimentally. The proposed models quantify the combined effects of multilayer textile geometry and additional ventilation, including airflow rate, supplied air temperature, and microclimate thickness, on airflow and heat dissipation. The numerically predicted AP, thermal resistance, effective thermal conductivity, and heat transfer coefficients were compared with values reported in the literature. Mesh-convergence analysis confirmed numerical stability and mesh-independent results. In addition, an extended ventilation model was developed to evaluate the influence of forced airflow and supplied air temperature on heat extraction from the skin to the textile structure. All simulations were performed using COMSOL Multiphysics software, and postprocessing was carried out using MATLAB software.

The structure of the article is as follows. The second section describes the textile geometries, governing equations, and boundary conditions for AP and thermal resistance modeling. In addition, it provides details about mesh generation and convergence procedures. The following section presents the validated AP results, the thermal performance metrics for Models 1–3, and the additional ventilation model outcomes. The final section summarizes the main conclusions and limitations.

Mathematical formulation of the problem

Materials

In this investigation, the unit cell geometry was based on the experimental findings of Zupin et al.,[27] where single-layer woven fabrics were evaluated by measuring their structural parameters and AP coefficient (see Table 1). Measurements of the AP coefficient were conducted using an FX 3300 Labotester III AP tester (Textest Instruments) in accordance with the ISO 9237:1995(E) standard.[11,27] The proposed unit cell was used as a representative volume element (RVE) for the woven fabric (see Figure 1). The unit cell was defined as a square domain with in-plane dimensions $L_x = L_y = 0.984$ mm, $L_z = 0.466$ mm. The unit cell should be interpreted as a close-to-real (equivalent) square plain-woven microstructure that preserves the measured fabric thickness and porosity. Porosity and local permeability were selected from the investigation done by Pezzin.[28] In the textile domain, two warp and two weft yarns are arranged in a plain-weave pattern and modeled as interlacing elliptical yarn segments. The RVE consists of two domains: Ω_1 (air domain) and Ω_2 (textile domain).

The proposed unit cell model was extended to an idealized geometrical model of a plain-woven 3D textile model (see Figure 2). The 3D textile structure (spacer fabric) may be woven, nonwoven, braided, or knitted. Woven spacer fabrics are another type of multilayered textile that has two outer layers produced by two independent warp systems, with an additional warp system that moves through the outside layers to form a 3D-spaced fabric.[29] The size of the air domain varies based on which coefficient is numerically predicted. This

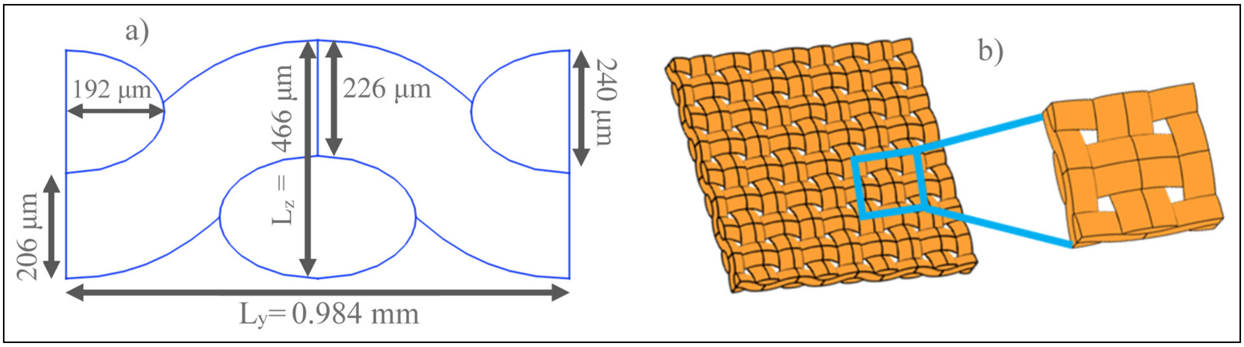

Figure 1. (a) Schematic diagram of yarn measurement parameters. (b) Unit cell domain of a single-layer textile domain.

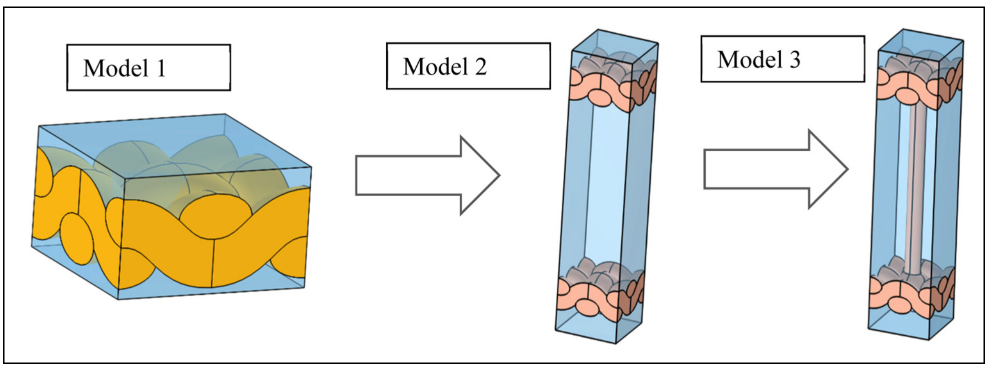

Figure 2. Representative volume element that consists of an air and a textile domain in the case of a one-layer structure (Model 1), two-layer structure (Model 2), 3D textile (spacer fabric) (Model 3).

study examined three models: one-layer (Model 1), two-layer (Model 2), and a 3D textile structure (Model 3) (see Figure 2).

Mathematical formulation of the AP model

The AP was simulated under the following assumptions.

1. The air flow is isothermal, incompressible, and steady state.
2. The Reynolds number (*Re*) is less than 2300, indicating that the flow is laminar. It should be noted that the *Re* was obtained from experimental data[27] of the sample plain weave (PL) 29.3/15 and is approximately 12.7.
3. The fluid is air and is considered a single-phase Newtonian fluid.

The AP (air flow) of textile structures was modeled by applying the momentum Navier–Stokes equation

$$\rho(\boldsymbol{u}\cdot\nabla)\boldsymbol{u} = \nabla\cdot\left[-p\boldsymbol{I} + \mu\left(\nabla\boldsymbol{u} + (\nabla\boldsymbol{u})^{\mathrm{T}}\right)\right] + \boldsymbol{F}\,\mathrm{in}\,\Omega_1 \qquad (1)$$

and the Brinkman equation

$$\frac{\rho}{\varepsilon_p}\left((\boldsymbol{u}\cdot\nabla)\frac{\boldsymbol{u}}{\varepsilon_p}\right) = \nabla\cdot\left[-p\boldsymbol{I} + \frac{\mu}{\varepsilon_p}\left(\nabla\boldsymbol{u} + (\nabla\boldsymbol{u})^T\right)\right.$$
$$\left. - \frac{2}{3}\frac{\mu}{\varepsilon_p}(\nabla\cdot\boldsymbol{u})\boldsymbol{I}\right] - \left(\mu k^{-1}\right)\boldsymbol{u} + \boldsymbol{F}\,\mathrm{in}\,\Omega_2 \qquad (2)$$

as well as the mass continuity equation[30,31]

$$\rho\nabla\cdot(\boldsymbol{u}) = 0\,\mathrm{in}\,\Omega_1\ \mathrm{and\ in}\ \Omega_2 \qquad (3)$$

where $\boldsymbol{u}$ stands for the velocity vector of the fluid in meters per second, p is pressure in pascals, μ is the dynamic viscosity of the fluid in pascal seconds, ρ is the density of fluid in kilograms per cubic meter, $\boldsymbol{I}$ is the identity matrix, $\boldsymbol{F}$ is the external force vector (in this case, equal to zero), ε_p is the porosity of yarns, and k is the local permeability coefficient of the porous media. Equation (1) contains the inertia term $(\boldsymbol{u}\cdot\nabla)\boldsymbol{u}$, a divergence of the stress term is $-p\boldsymbol{I} + \mu\left(\nabla\boldsymbol{u} + (\nabla\boldsymbol{u})^{\mathrm{T}}\right)$, and $-\nabla p\boldsymbol{I}$ represents the pressure difference forces.[32]

The Brinkman equation (2) requires porosity and local AP coefficients.[31] Those are the most important attributes for predicting AP. Local permeability assesses the ability of a porous material (textile) to transport fluids.[33] It might be evaluated using

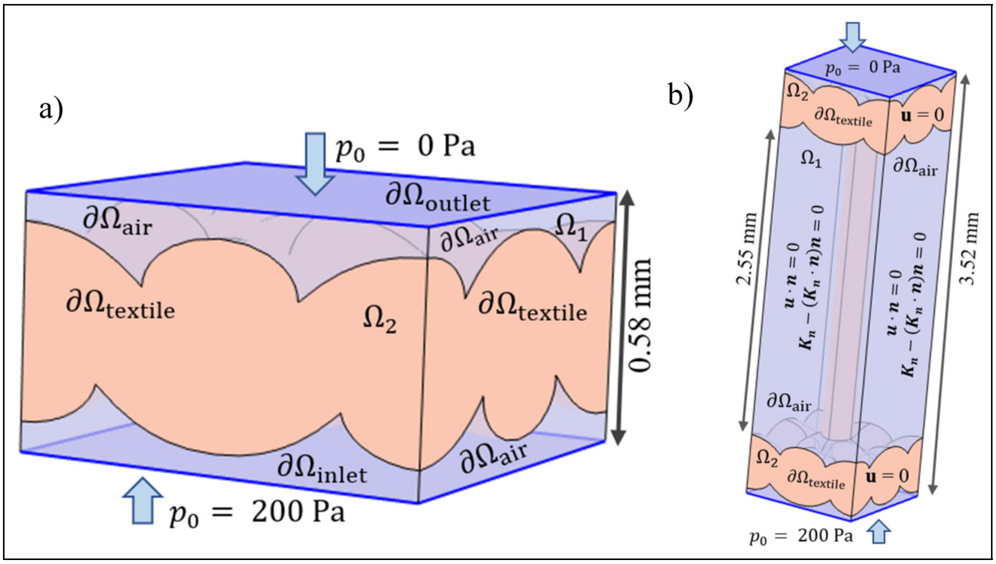

Figure 3. Boundary conditions of AP test for (a) Model 1 and (b) Model 3.

analytical methods such as those described by Gebart[34] and Kozeny-Carman.[35] These methods explain the relationship between permeability and porosity. Several authors[36-38] have investigated the dual-scale permeability problem numerically using the Stokes or Stokes–Darcy approaches. The local AP k of polyester yarn is reported to be between 1.53×10^{-12} and 8.20×10^{-11} m^2 according to the literature.[38] This study employed a textile structure porosity ε_p of 0.58, and the square AP k was determined to be 1.35×10^{-11} m^2.[28]

The inlet boundary condition corresponds to ISO 9237:1995, specifying a pressure difference of 200 Pa:[11,27]

$$\boldsymbol{n}^T\left[-p\boldsymbol{I} + \mu\left(\nabla\boldsymbol{u} + (\nabla\boldsymbol{u})^T\right)\right]\boldsymbol{n} = -\hat{p}_0, \quad \hat{p}_0 \geqslant p_0,$$
$$\boldsymbol{u}\cdot\boldsymbol{t} = 0, \; p_0 = 200 \text{ Pa on } \partial\Omega_{\text{inlet}} \tag{4}$$

where $\boldsymbol{n}$ is the outer unit normal vector, and $\boldsymbol{t}$ is the tangential vector. The outlet boundary condition is a pressure of 0 Pa, which represents atmospheric pressure

$$\left[-p\boldsymbol{I} + \mu\left(\nabla\boldsymbol{u} + (\nabla\boldsymbol{u})^T\right)\right]\boldsymbol{n} = -\hat{p}_0\,\boldsymbol{n}, \; \hat{p}_0 \leqslant p_0,$$
$$p_0 = 0 \,\text{Pa on } \partial\Omega_{\text{outlet}} \tag{5}$$

A no-slip boundary condition was applied to all textile surfaces, ensuring a zero air velocity at the yarn–air interfaces

$$\boldsymbol{u} = 0 \text{ on } \partial\Omega_{\text{textile}} \tag{6}$$

Slip wall conditions were implemented at the external boundaries of the surrounding air domain

$$\boldsymbol{u}\cdot\boldsymbol{n} = 0, \; \boldsymbol{K_n} - (\boldsymbol{K_n}\cdot\boldsymbol{n})\boldsymbol{n} = 0 \text{ on } \partial\Omega_{\text{air}} \tag{7}$$

The boundary conditions are illustrated in Figure 3. First-order Lagrange finite elements were employed to discretize the incompressible laminar flow equations in both the free-fluid and porous (Brinkman) domains. A stabilized P1–P1 formulation was used to solve the flow problem, which applies linear basis functions to velocity and pressure.[30,31,39]

In (7), $\boldsymbol{K_n} = \boldsymbol{Kn}$. For the air domain Ω_1, the viscous stress tensor is expressed as $\boldsymbol{K} = \mu\left(\nabla\boldsymbol{u} + (\nabla\boldsymbol{u})^T\right)$. In the porous (Brinkman) domain Ω_2, the volume-averaged viscous stress tensor is defined as $\boldsymbol{K} = \frac{\mu}{\varepsilon_p}\left(\nabla\boldsymbol{u} + (\nabla\boldsymbol{u})^{\mathrm{T}}\right) - \frac{2}{3}\frac{\mu}{\varepsilon_p}(\nabla\cdot\boldsymbol{u})\boldsymbol{I}$. In the case of incompressible flow $(\nabla\cdot\boldsymbol{u}) \approx 0$ and the correction term $-\frac{2}{3}\frac{\mu}{\varepsilon_p}(\nabla\cdot\boldsymbol{u})\boldsymbol{I}$ vanishes.

The airflow modeling was done using the *Laminar Flow* interface, and the porous textile regions were represented using the *Porous Medium Domain* formulation based on the Brinkman equations.

Mathematical formulation of the thermal resistance model

The thermal characteristics of the textile structures were modeled based on the assumption of no heat transfer by convection or radiation. Radiation was neglected due to a small temperature gradient.[40,41]

The material properties of the textile are presented in Table 2. The axial thermal conductivity of yarn (K_{ya}) was determined using the parallel model

$$K_{\text{ya}} = K_{\text{fl}}V_{\text{fy}}K_{\text{air}}\left(1 - V_{\text{fy}}\right) \tag{8}$$

Yarn transverse thermal conductivity $\left(K_{\text{yt}}\right)$ was estimated by the series model[43]

$$K_{\text{yt}} = \frac{K_{\text{ft}}K_{\text{air}}}{V_{\text{fy}}K_{\text{air}} + K_{\text{ft}}\left(1-V_{\text{fy}}\right)} \tag{9}$$

Table 2. Thermal physical properties of polyester fibers.[42]

Material	Density (kg/m^3)	Heat capacity (kJ/kg·K)	Thermal conductivity (W/m·K)
Polyester	1390	1030	1.260 (longitudinal K_{fl}) 0.157 (transverse K_{ft})

It should be noted that K_{fl} is the thermal conductivity along the fiber axis, K_{ft} denotes thermal conductivity perpendicular to the fiber axis, V_{fy} stands for the fiber volume fraction of yarn, and K_{air} is the thermal conductivity of air.[44] The local thermal conductivity tensor K for the yarn is defined as follows, with the thermal conductivity of the yarn along the fiber ($K_{11} = K_{ya}$) and transverse ($K_{22} = K_{33} = K_{yt}$) to fiber direction:[45]

$$K = \begin{bmatrix} K_{11} & 0 & 0 \\ 0 & K_{22} & 0 \\ 0 & 0 & K_{33} \end{bmatrix} \tag{10}$$

Experimentally, the thermal resistance of textiles can be examined with the Sweating Guarded Hot Plate M259B apparatus in accordance with ISO 11092,[7] which is usually referred to as the "skin model." This approach facilitates the realistic imitation of heat and mass transfer processes that take place next to human skin under steady-state conditions.[7,9] The thermal resistance of a textile is defined as the temperature difference between two faces of a material (T_m and T_a) divided by the resultant heat flux H per unit area A in the direction of the gradient

$$R_{ct} = \frac{(T_m - T_a)A}{H - \Delta H_c} - R_{ct0} \tag{11}$$

where T_m is the mean temperature of the measuring unit in kelvin, T_a is the air temperature in the test enclosure in kelvin, H is the heating power in watts required to maintain the plate temperature at $T = 35°C$, ΔH_c is the correction term for the heating power, R_{ct0} is the apparatus constant in square meter kelvin per watt, for the measurement of thermal resistance without a sample.[7] The thermal resistance measurement process includes setting the measuring unit temperature to $T_m = 35.0°C$ and the ambient air temperature to $T_a = 20.0°C$, and the relative humidity is automatically regulated to 65%.[7,9] The effective thermal conductivity (K_{eff}) can be obtained from

$$K_{eff} = \frac{L_z}{R_{ct}} \tag{12}$$

and the heat transfer coefficient from[9]

$$h_{eff} = \frac{1}{R_{ct}} \tag{13}$$

Thermal resistance (R_{ct}), effective heat transfer (h_{eff}), and effective thermal conductivity (K_{eff}) coefficients of the textile structures were modeled utilizing the energy equation[31]

$$\rho C_p \boldsymbol{u} \cdot \nabla T + \nabla \cdot \boldsymbol{q} = Q, \ \boldsymbol{q} = -K\nabla T \ \text{ in } \Omega_1 \text{ and } \Omega_2 \tag{14}$$

where C_p is the specific heat capacity in joules per kilogram per kelvin, Q is the overall heat transfer in watts, T is the temperature in kelvin, and K represents the thermal conductivity of the fluid–solid mixture in watts per meter per kelvin. It should be noted that K is the local thermal conductivity of the fluid–solid mixture and was obtained from (10) and applied to the Ω_2 domain. The boundary conditions were selected in accordance with ISO 11092:2014 (EN)[7] and are depicted in Figure 4.

Thermal resistance modeling was performed using the *Heat Transfer in Solids and Fluids* interface in COMSOL Multiphysics software.

Additional ventilation model for a 3D woven spacer textile

The AP and thermal resistance models described in the last two subsections, in which the textile domains are a porous medium, represent transport through the thickness under constant pressure and temperature gradients in a stationary configuration. However, advanced protective clothing systems often include forced airflow channels that provide additional ventilation and thus affect the local heat and mass transfer in the textile layer.[21,46,47] The current additional ventilation model is based on a previously developed microscale forced-ventilation model.[48] In this study, the extended model retains the same porous 3D woven spacer structure, and an external airflow is added to analyze forced convection. When the human body is wearing cold-protective clothing and exposed to windy conditions, the dominant heat-loss mechanisms are conduction within the textile and convection caused by ventilation, while radiative exchange is relatively small.[6] For this reason, the radiative heat transfer is neglected in this investigation.

The additional ventilation model is carried out under the assumptions that heat transfer occurs due to convection (there is air movement) and conduction, and the air flow is identified as nonisothermal,

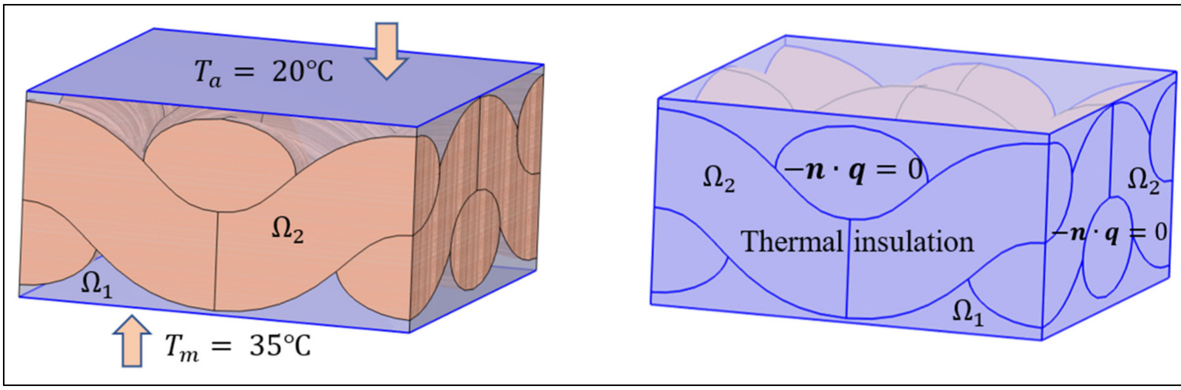

Figure 4. Boundary conditions of thermal resistance.

incompressible, and steady state. The governing equations include a set of Navier–Stokes[30] and Brinkman equations[31] (1)–(3) and the energy equation[31] (14). Boundary conditions are illustrated in Figure 5. The additional ventilation model was developed to represent forced air exchange through the textile and air domain under controlled inlet flow conditions. A standard volumetric flow rate Q_{sv} was specified at the inlet boundary ($\partial\Omega_{inlet}$) using an integral mass-flow formulation, in which the imposed flow rate varied between 0 and 0.5 dm^3/min, and is referenced to standard conditions through the standard density.[39] At the specified flow rates, the resulting Reynolds number ($Re < 2300$) remains within the laminar regime. At the outlet boundary ($\partial\Omega_{outlet}$), a pressure outlet condition was applied with the ambient reference pressure $p_0 = 0$ Pa (see (5)). Wall no-slip conditions (6) were imposed on the yarn surfaces (on $\partial\Omega_{textile}$) and the skin surface to ensure the physical wall constraint and correctly capture near-wall momentum losses. Wall slip conditions (7) were set for the surrounding air surfaces (on $\partial\Omega_{air}$). In the thermal problem, the human skin was represented by a constant temperature boundary condition ($T_{skin} = 37°C$), whereas the outlet was associated with ambient temperature ($T_a = 20°C$). Two inlet air temperature scenarios were considered at the $\partial\Omega_{inlet}$ boundary, where the supplied air temperature T_b was set to 10°C and 20°C. All other external boundaries were thermally insulated.

An additional parametric analysis was performed in which the textile domain was simplified as a solid domain without porous flow (i.e., the Brinkman equation[31] (2) was not applied), allowing the geometric effect of the microclimate thickness to be isolated from porous transport effects. In this case, airflow in the microclimate layer was governed by the Navier-Stokes equations[30] (1) and (3), coupled with the energy equation (14). The thickness of the microclimate (air gap between skin and textile) layer was systematically

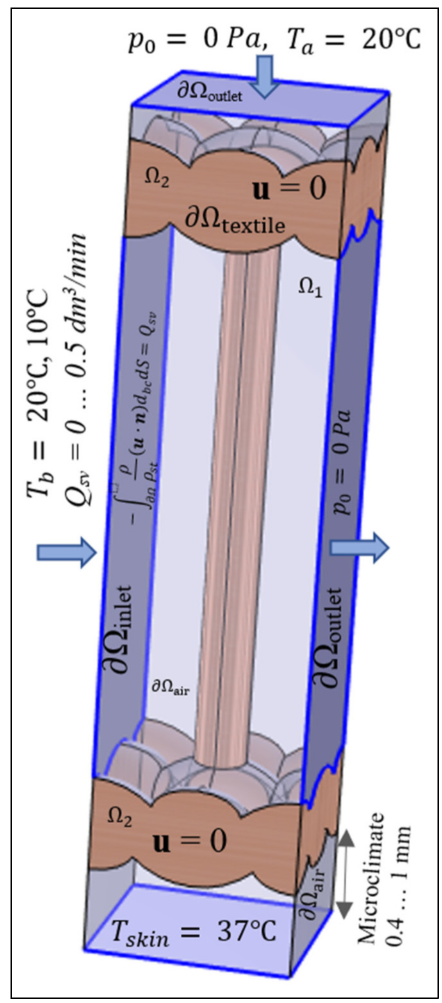

Figure 5. Computational domain and boundary conditions for the additional ventilation model.

varied in the range 0.4–1 mm in order to quantify its effect on the microclimate airflow and the resulting temperature field. Specifically, the parametric sweep was used to assess how changes in air gap thickness

Table 3. Specification of the mesh used for the prediction of the AP of Model 1.

Total number of elements	8763	9533	16,277	33,407	58,090	186,036	509,475
Minimum element quality	0.138	0.123	0.123	0.147	0.091	0.112	0.097
Average element quality	0.611	0.618	0.635	0.659	0.668	0.678	0.684

Table 4. Specification of the mesh used for the prediction of the thermal resistance of Model 1.

Total number of elements	6084	7810	10,211	17,637	33,988	64,626	175,971	482,310
Minimum element quality	0.024	0.053	0.091	0.108	0.065	0.103	0.069	0.038
Average element quality	0.588	0.598	0.609	0.619	0.636	0.643	0.650	0.655

affect ventilation effectiveness and, consequently, the microclimate temperature.

An additional ventilation model was created using the *Laminar Flow and Heat Transfer in Solids and Fluids* interfaces, which were coupled with the *Nonisothermal Flow* interface.

Configuration of mesh

In this study, three models were built with COMSOL Multiphysics software.[39] The quality of the mesh element was evaluated using the skewness metric

$$1-\max\left(\frac{\theta-\theta_e}{180-\theta_e}\ ,\ \frac{\theta_e-\theta}{\theta_e}\right) \tag{15}$$

where θ is the angle over a vertex (2D) or edge (3D) in the element, θ_e is the angle of the corresponding vertex or edge in an ideal element, and the minimum is taken over all vertices (2D) or edges (3D) of the element.[39] The equiangular skewness metric assigns a penalty to elements with internal angles that are extremely large or small relative to the angles of an ideal element.[39,49] The corresponding quality of the mesh element is expressed as a dimensionless quantity in the range from 0 to 1, where skewness close to 1 denotes a perfectly regular element and 0 represents a degenerate element. Mesh elements with a quality close to 0.01 are generally considered to be of extremely low quality and are usually avoided in critical regions of the domain due to their potential to cause solver convergence issues.[39]

In this investigation, different mesh sizes were employed for Model 1 (one-layer textile) in order to identify the optimal number of elements. The air domain height of 0.58 mm was used to predict AP, and a minimal air domain height of 0.5 mm was applied to predict the thermal resistance, effective thermal conductivity, and effective heat transfer coefficient. Tables 3 and 4 present the total number of elements, as well as the minimum and the average element quality.

After several iterative mesh refinements, the RVE of Model 2 was created from 510,663 elements with an average element quality of 0.664 and a minimum element quality of 0.0224. The RVE of Model 3 consisted of 525,596 domain elements with an average element quality of 0.660 and a minimum element quality of 0.0221. Figure 6 depicts the mesh utilized for Model 3 (which had a microclimate layer and was used in an additional ventilation simulation), along with the corresponding skewness quality metric. The air domain height of 4 mm was applied for Model 3. The height of the microclimate layer was set to 0.4 mm.

Computational setup

All numerical simulations were carried out on a computational workstation equipped with a 13th-generation Intel Core i7-13700H processor and 16 GB RAM. COMSOL Multiphysics version 6.2 was run on the Windows operating system, utilizing up to 10 CPU cores for calculations. The governing equations were discretized using first-order Lagrange finite elements. The stationary systems were solved using a fully coupled approach with Newton iterations[50] and the PARDISO direct linear solver.[51] Postprocessing was performed using MATLAB R2024a, whereas the graphical visualization of the results was prepared using OriginPro 2026.

Results and discussion

Mesh-convergence analysis was conducted for Model 1 by increasing the total number of elements and evaluating the corresponding changes in the predicted AP and effective thermal conductivity. It was found that the effective thermal conductivity of a one-layer textile made from polyester varies from 0.03242 to 0.03274 W/m·K (see Figure 7). Figure 7 demonstrates that the numerically predicted effective thermal conductivity for coarse meshes initially increases rapidly, but with the

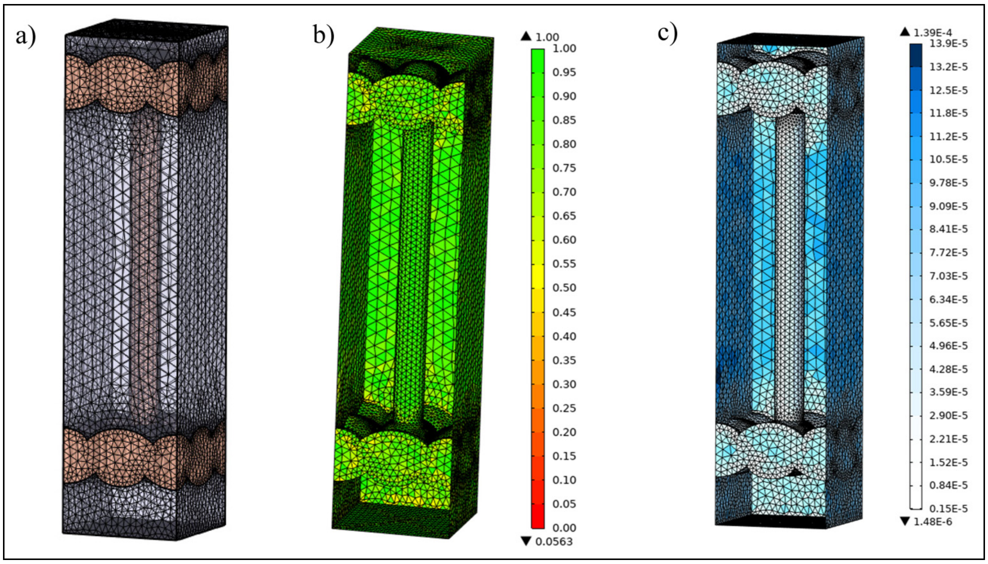

Figure 6. (a) Illustration of the volumetric mesh of Model 3. (b) The mesh quality, evaluated based on the skewness metric. (c) The distribution of mesh element sizes, in meters.

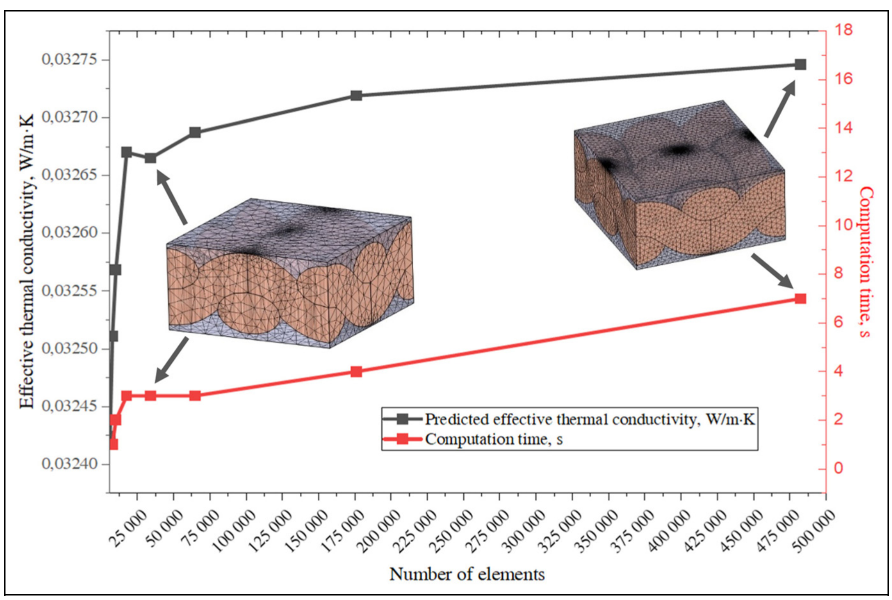

Figure 7. Mesh-refinement study illustrating the convergence of the predicted effective thermal conductivity.

further refinement of the total number of elements, the values of K_{eff} are stable, reflecting numerical convergence. The results indicate that refining the mesh beyond 64,626 elements leads to only insignificant changes in K_{eff}, while the computational time continues to increase. This highlights a clear trade-off between accuracy and computational cost, justifying the selection of an intermediate mesh size where K_{eff} is 0.032687 W/m·K and has already reached a stable value. The numerically predicted effective thermal conductivity (0.032687 W/m·K) is in the same range as the values of polyester fabrics reported in the literature[52] (0.03152–0.04230 W/m·K, numerically predicted, and 0.0350–0.0403 W/m·K, experimentally measured), indicating a good agreement despite the different textile architectures. The observed difference can be explained by the structural differences between woven and knitted fabrics, including differences in yarn trajectory, porosity, and contact areas at crossover or loop junctions. In this study, it was found that the thermal resistance of

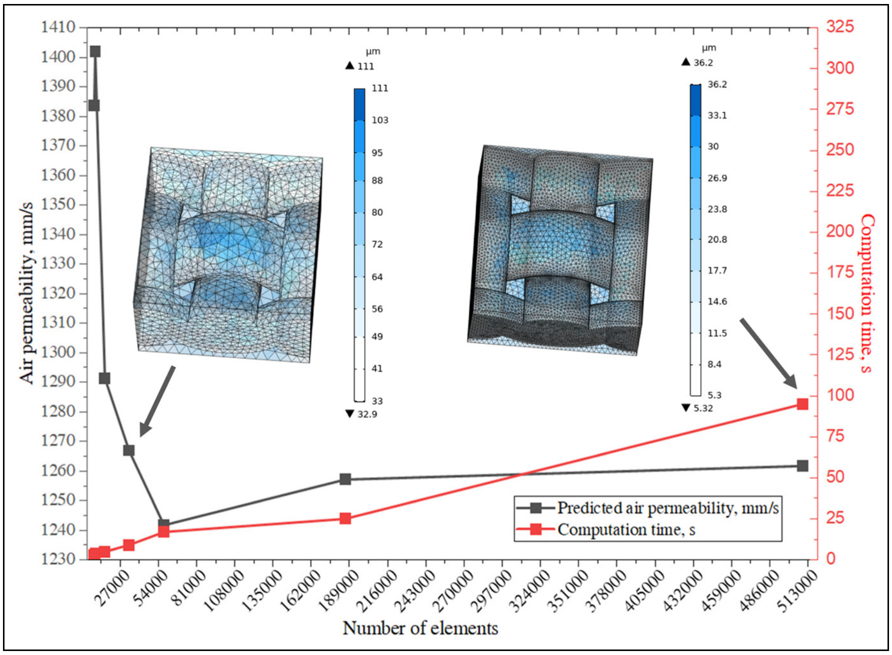

Figure 8. Mesh-refinement study illustrating the convergence of the predicted AP.

one-layer polyester textile is 0.014427 m^2 K/W, and the corresponding conductive heat transfer coefficient is 70.145 W/m^2 K.

Figure 8 depicts a mesh convergence analysis of Model 1, showing the relationship between the predicted AP and the total number of elements, along with the corresponding computation time. The results indicate that coarse meshes lead to an overestimation of AP, reaching values of up to 1401.9 mm/s. When the mesh is too coarse, it may not accurately resolve the velocity gradients that occur near the wall region around the yarn surfaces (no-slip boundaries). This may result in the incorrect estimation of the pressure drop and AP. As the mesh is refined, the predicted permeability decreases significantly, reaching a minimum of 1241.7 mm/s at 58,090 elements. Further refinement to 186,036 and 509,475 elements results in only minor variations in the predicted AP, which stabilizes at 1257.1 and 1261.7 mm/s, respectively. These values correspond to a relative error of approximately 0.5%–2.1% compared with the experimental value reported in literature.[27] This demonstrates that the solution has become independent from the mesh. In contrast, the time required to compute AP increases with the number of elements and becomes significantly longer, up to 95 s for the mesh that contains 509,475 elements. The mesh size visualizations (see Figure 8) illustrate that the coarse mesh has a much larger element size, ranging from approximately 32.9 to 111 μm, whereas the refined mesh employs considerably smaller elements, ranging from approximately 5.32 to 36.2 μm, which improves resolution but increases computational cost. The converged AP coefficients also align well with previously experimentally measured values for similar one-layer woven structures. According to the literature,[27] the AP is 1268.33 mm/s at a pressure drop of 200 Pa, while the numerically predicted AP is 1257.1 mm/s. This indicates a good agreement for the considered case. Figure 9 provides additional information for the airflow predictions by displaying the pressure and velocity fields in Model 1. The pressure decreases monotonically throughout the thickness, while the velocity is highly concentrated at the pore openings, forming jet-like regions that dominate the airflow.

Table 5 summarizes the predicted AP coefficient, effective thermal conductivity, heat transfer coefficient, and thermal resistance for three polyester architectures: Model 1 (one-layer), Model 2 (two-layer), and Model 3 (3D textile). Model 1 has the highest AP (1257.1 mm/s) and the lowest thermal resistance (R_{ct} = 0.0144 m^2 K/W), and the largest conductive heat transfer coefficient (h_{eff} = 70.145 W/m^2 K). On the other hand, when a second layer is added (Model 2), the transportation paths become much more limited. The AP decreases to 448.39 mm/s (2.80 times lower), while thermal resistance increases to 0.12537 m^2 K/W (8.69 times higher). It is important to highlight that the K_{eff} value decreases by 14.1%, indicating that the main factor that influences the thermal resistance value is related to textile geometry, such as increased complexity of heat flow paths, a larger proportion of stagnant air, and less effective solid connections through the thickness. The Model 3 results are almost the same as those of Model 2, with

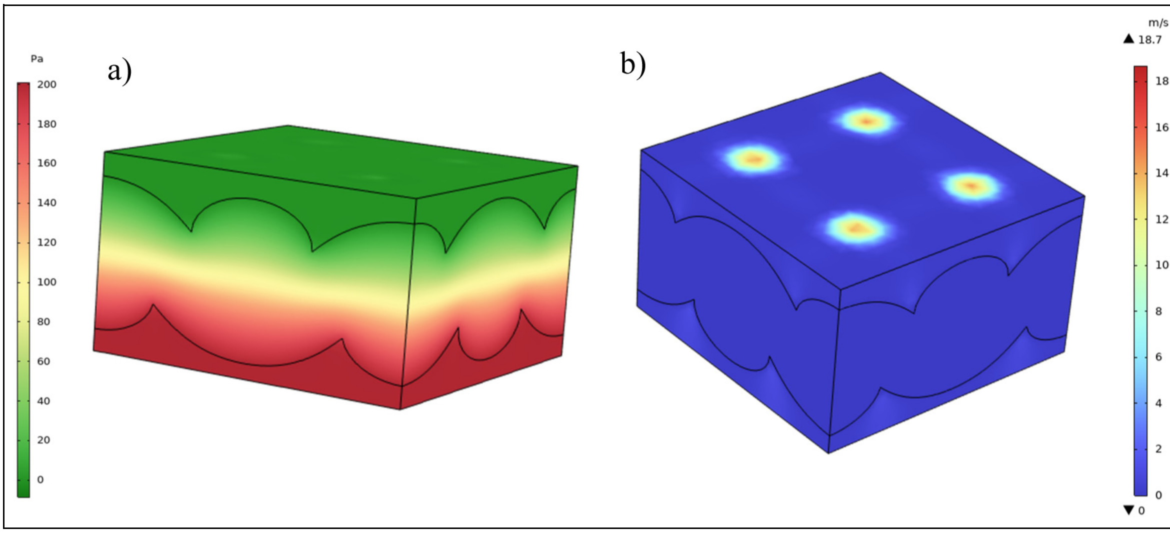

Figure 9. Distribution of (a) pressure and (b) velocity fields in Model 1.

Table 5. Summary of numerically predicted AP and thermal performance metrics.

Model	AP (mm/s)	Effective thermal conductivity K_{eff} (W/m·K)	Thermal resistance R_{ct} (m^2 K/W)	Heat transfer coefficient h_{eff} (W/m^2 K)
Model 1	1257.1	0.032687	0.014427	70.145
Model 2	448.39	0.028077	0.12537	7.9765
Model 3	447.91	0.028552	0.12328	8.113

differences in thermal performance that are less than 2% for thermal metrics and 0.1% for AP. In a comparison between Model 3 and the experimental 3D textile layer reported in the literature[47] (which measured an AP of 404 mm/s, a thermal resistance of 0.118 m^2 K/W, and obtained a corresponding heat transfer coefficient of 8.4746 W/m^2 K), Model 3 predicts a 10.87% higher AP and 4.47% higher thermal resistance coefficient. The remaining differences are expected, as AP and thermal resistance in 3D textile structures are influenced by the topology, distance between layers, layer alignment, and thickness. Furthermore, standardized testing introduces attributes such as fabric compaction, thickness variations, imperfect plate contact, and edge effects that can lower measured AP and impact thermal resistance.[53,54] These effects are difficult to reproduce exactly in an idealized computational model. Nevertheless, the good agreement of the absolute values confirms the validity of the proposed computational models. Figure 10 illustrates the corresponding 3D temperature field distributions for the investigated polyester architectures under pure thermal conductivity, providing a qualitative validation of the differences reported in Table 5.

Figure 11 depicts the convergence behavior of the fully coupled nonlinear stationary solver for the 3D textile AP model. The solution error estimate for the velocity field decreased from 1.2 to 2.7 $\times$ 10^{-6}, while the pressure solution error decreased from 0.87 to 1.3 $\times$ 10^{-8}. In addition, the velocity residual error dropped from 490 to 5.3 $\times$ 10^{-5}, whereas the pressure residual error decreased from 7200 to 1.5 $\times$ 10^{-3}. The overall reduction of the solution and residual errors by several orders of magnitude indicates the convergence and numerical stability of the 3D textile AP simulation. This simulation required approximately 349 s of wall-clock time, corresponding to about 0.97 CPU hours on a 10-core Intel-based workstation using the PARDISO direct solver.

An additional ventilation model was developed to evaluate the impact of forced airflow in the microclimate layer on heat transfer from the skin–textile system. Ventilation was applied at a specified standard flow rate (Q_{sv} = 0–0.5 dm^3/min), corresponding to average inlet velocities of approximately 0.14, 1.43, and 3.59 m/s for 0.02, 0.2, and 0.5 dm^3/min, respectively, and two supply air temperatures (T_b = 20°C and T_b = 10°C) were evaluated. Table 6 demonstrates that forced ventilation strongly enhances heat transfer and reduces the thermal resistance of the skin–textile system. In the no-ventilation case, the heat transfer coefficient is low (h_{eff} = 7.14 W/m^2 K), resulting in the highest thermal

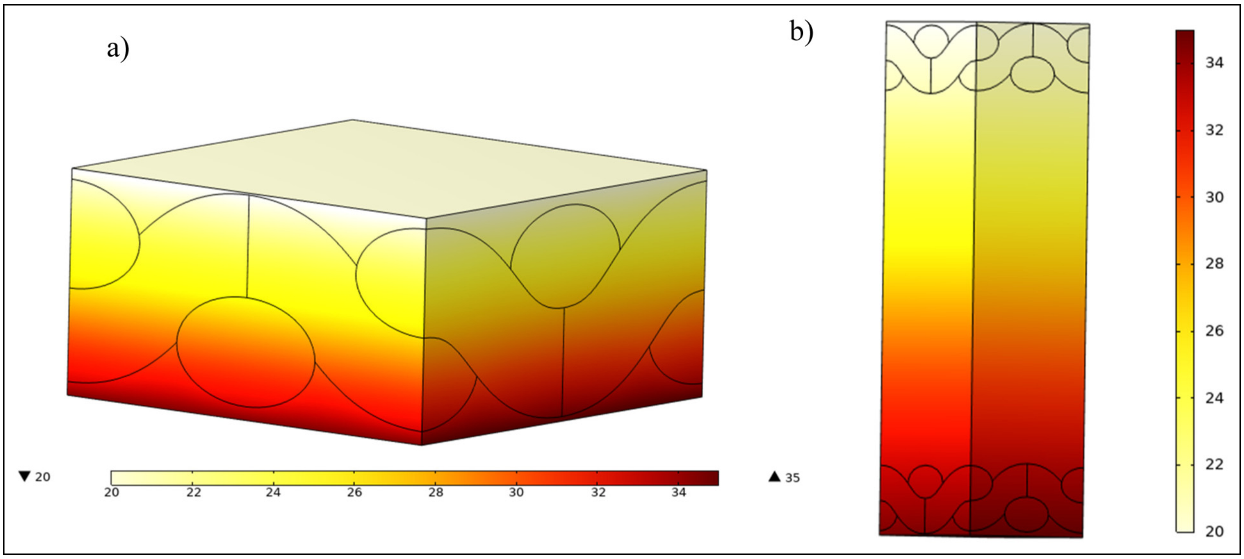

Figure 10. Volumetric temperature field in (a) Model 1 and (b) and Model 2 under pure heat conduction. The color scale (20–35°C) depicts the through-thickness temperature gradient, with higher temperatures closer to the bottom boundary (skin) and lower temperatures toward the top boundary.

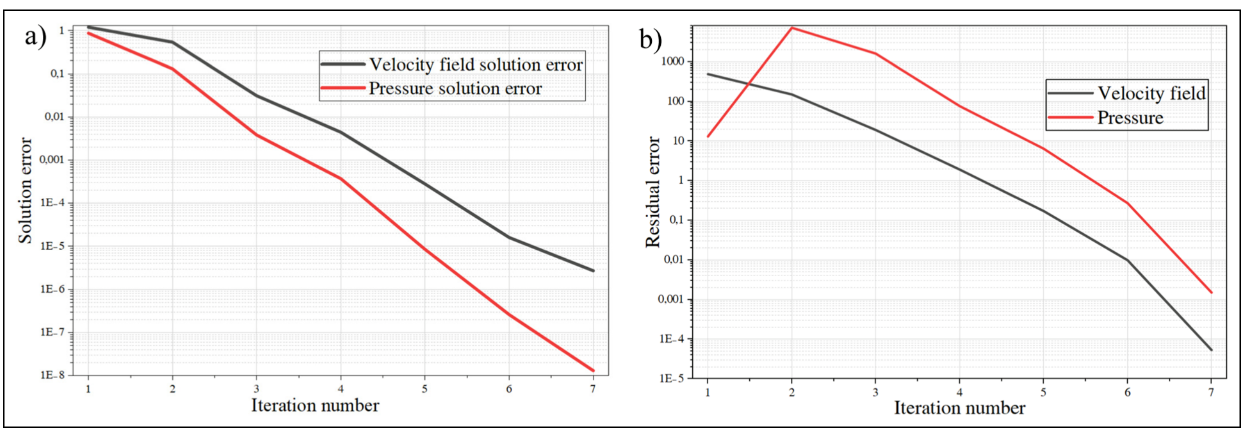

Figure 11. Convergence plots of the fully coupled nonlinear stationary solver: (a) solution error estimates for dependent variables and (b) residual error estimates for the velocity field and pressure during the iterations.

Table 6. Summary of numerically predicted heat transfer and thermal resistance coefficients.

Study case	Heat transfer coefficient h_{eff} (W/m^2 K)	Thermal resistance R_{ct} (m^2 K/W)
No ventilation	7.14	0.14
Q_{sv} = 0.02 dm^3/min, T_b = 20°C	27.52	0.036
Q_{sv} = 0.2 dm^3/min, T_b = 20°C	31.78	0.031
Q_{sv} = 0.5 dm^3/min, T_b = 20°C	33.69	0.029
Q_{sv} = 0.5 dm^3/min, T_b = 10°C	53.64	0.018

resistance (R_{ct} = 0.14 m^2 K/W). Even at low ventilation rates of 0.02 dm^3/min, thermal insulation is significantly reduced when airflow occurs. In this case, h_{eff} increases to 27.52 W/m^2 K and R_{ct} reduces to 0.036 m^2 K/W. When the air flow rate is increased to 0.2 dm^3/min, the h_{eff} value increases to 31.78 W/m^2 K. In addition, increasing the flow rate to 0.5 dm^3/min results in only a slight increase in the h_{eff} value (33.69 W/m^2 K). This behavior is consistent with previous observations that the loss of insulation from clothing during forced convection does not continue indefinitely, but approaches a

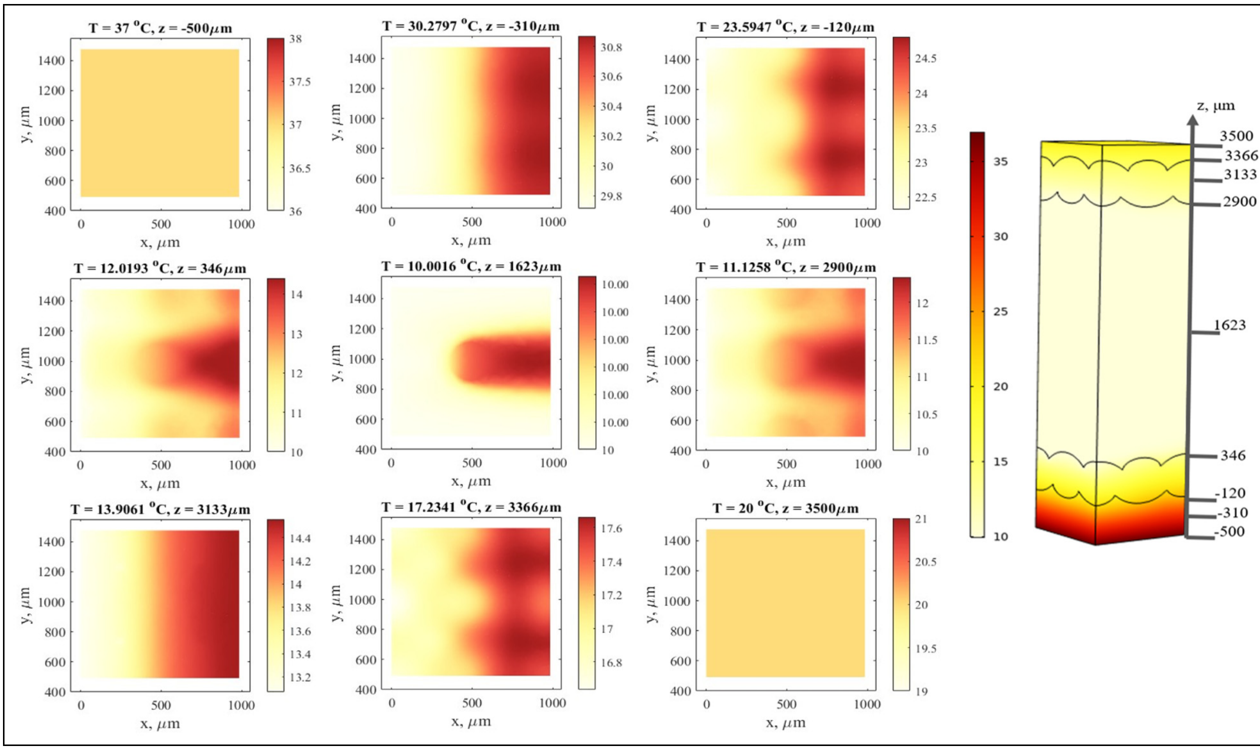

Figure 12. Cross-sectional temperature distribution in selected *z* planes for the ventilation model, where T_b = 10°C, Q_{sv} = 0.5 dm^3/min.

stable regime as the air movement increases.[55,56] Torres et al.[55] noted that, with increasing ambient air motion, air can penetrate into the microclimate through fabric pores and openings in the clothing system, thereby reducing the overall insulation.[55] These authors further reported that the insulation decrease associated with these mechanisms tends to plateau at wind speeds of approximately 3.5 m/s, although under certain conditions a similar effect can be observed at speeds as low as 2.0 m/s.[55] In the current ventilation model, the maximum flow rate is 0.5 dm^3/min combined with a reduced supplied air temperature (T_b = 10°C), resulting in the strongest cooling response, increasing h_{eff} to 53.64 W/m^2 K and reducing R_{ct} to 0.018 m^2 K/W. This indicates that when the airflow-induced insulation losses approach a plateau, additional cooling is more effectively achieved by reducing T_b rather than further increasing the ventilation rate.

Figures 12 and 13 illustrate cross-sectional temperature fields plotted on identical *x*–*y* axes at the same set of *z* locations along the textile domain. It should be noted that the *z*-axis indicator is included to specify the relative positions of the extracted planes from –500 μm (skin surface) to 3500 μm (outlet). At the ventilation rate Q_{sv} = 0.5 dm^3/min and at the T_b = 10°C case shown in Figure 12, the cooling is stronger across the domain, with downstream planes approaching the inlet air temperature (e.g., T = 10°C at z = 1623 μm and T = 12.02°C at z = 346 μm), whereas at the T_b = 20°C case (Figure 13), it remains close to 20–22°C in the corresponding sections (e.g., T = 20°C at z = 1623 μm and T = 21.30°C at z = 346 μm). In the middle of the microclimate layer at z = –310 μm, the predicted average temperature is T = 30.28°C for the T_b = 10°C case, compared with T = 32.78°C for the T_b = 20°C case, which is a 2.50°C lower temperature under the colder supplied air condition.

The same *z*-plane axis positions and identical in-plane axes were also used for the corresponding velocity distribution (Figures 14 and 15), enabling a direct comparison between flow localization and the resulting thermal field nonuniformity. The small differences in the velocity magnitudes between the T_b = 10°C and T_b = 20°C cases can be attributed to the temperature dependence of the air properties (ρ and μ) used in the flow model. It should be noted that the computational time for the ventilation simulation at Q_{sv} = 0.5 dm^3/min is approximately 974 s (2.71 CPU hours), indicating the computational feasibility of the proposed model.

Figures 16 and 17 show the effect of microclimate air gap thickness on the average temperature and velocity that were evaluated at the middle of the microclimate and at the upper microclimate boundary located directly in front of the first textile layer. In these parametric simulations, the textile was modeled as a solid domain (i.e., no porous flow resistance was included),

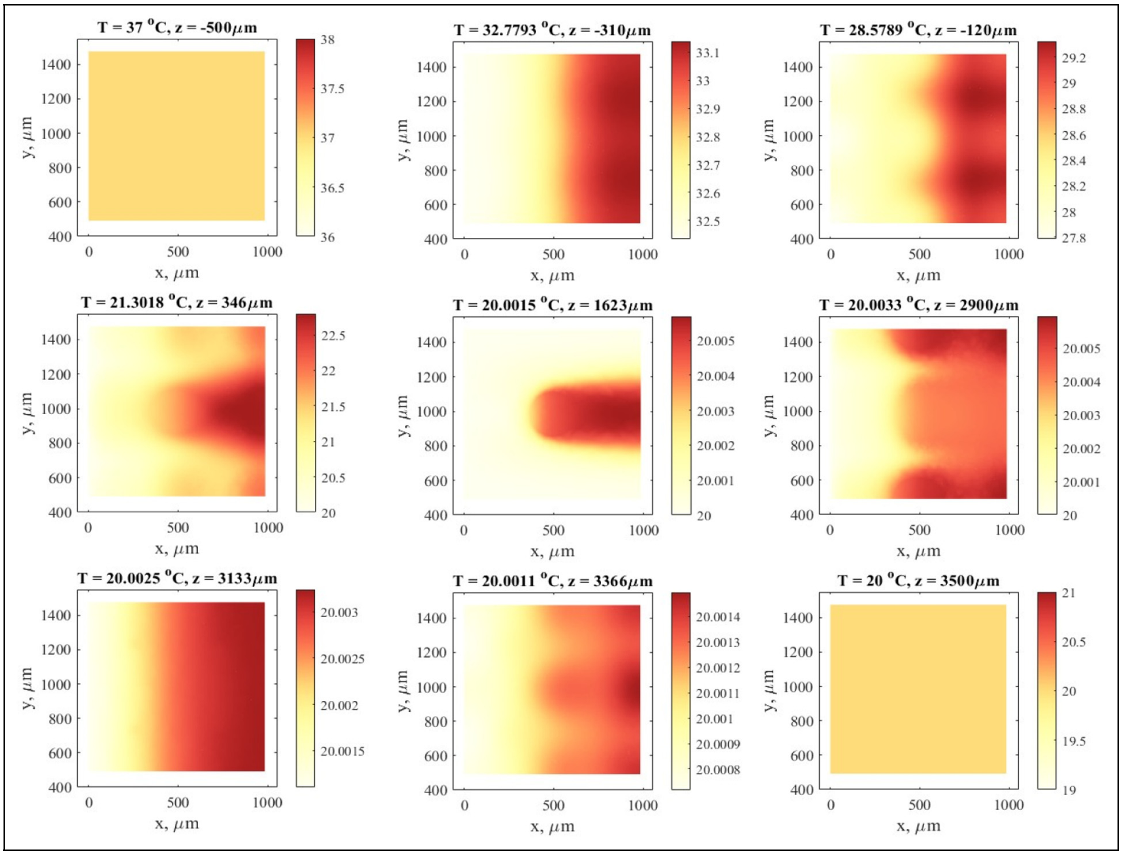

Figure 13. Cross-sectional temperature distribution in selected z planes for the ventilation model, where T_b = 20°C, Q_{sv} = 0.5 dm^3/min.

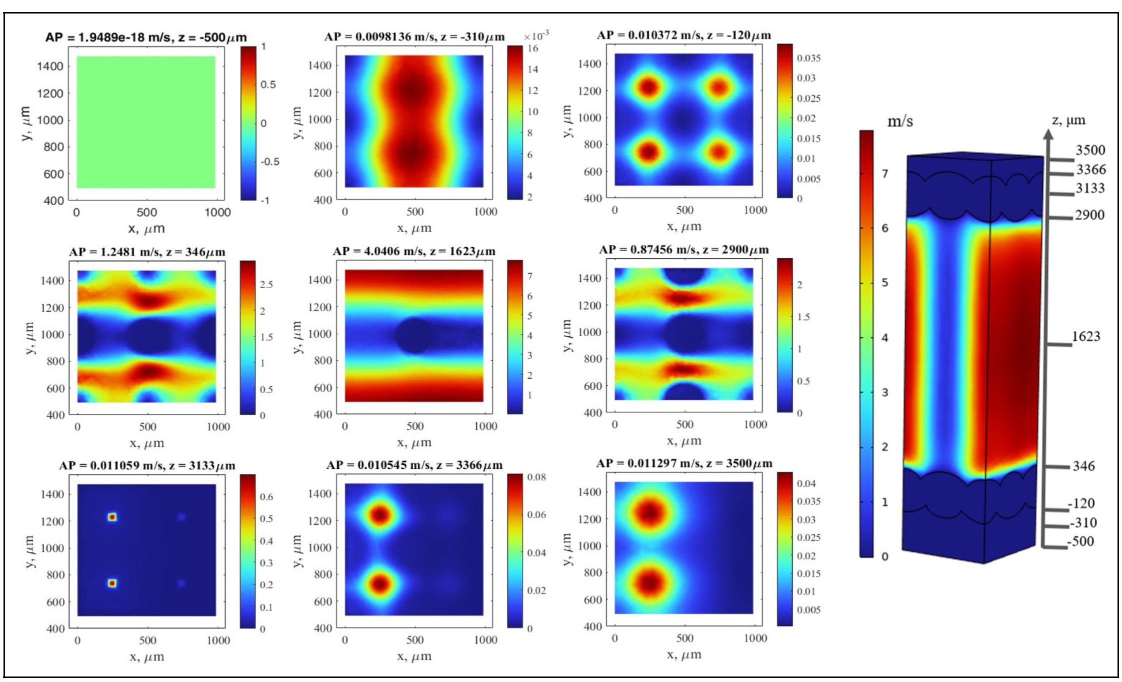

Figure 14. Cross-sectional velocity magnitude distribution in selected z planes for the ventilation model, where T_b = 10°C, Q_{sv} = 0.5 dm^3/min.

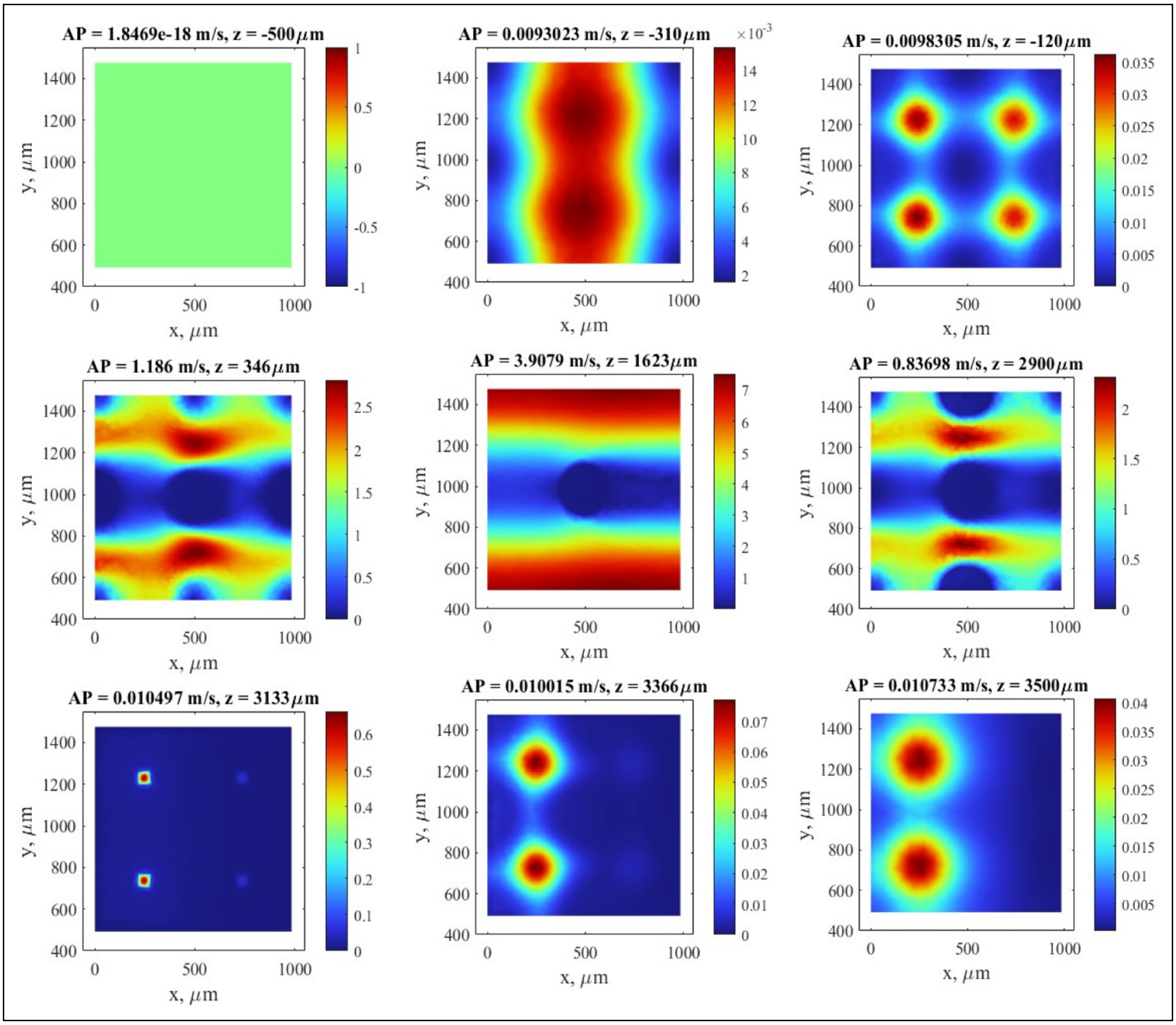

Figure 15. Cross-sectional velocity magnitude distribution in selected z planes for the ventilation model, where T_b = 20°C, Q_{sv} = 0.5 dm^3/min.

and the results are therefore intended to demonstrate the relative sensitivity to air gap thickness rather than provide absolute values for a specific fabric. As the air gap increases from 0.4 to 1.0 mm, the average temperature of the middle plane decreases from 32.82°C to 30.93°C, and the temperature close to the textile interface decreases even more from 28.64°C to 24.87°C (see Figure 16). This indicates enhanced cooling of the air adjacent to the textile with increasing microclimate thickness.

It was found that the average velocity at the upper boundary remains almost constant, varying from 3.64 to 3.44 mm/s, while the midplane velocity decreases significantly from 3.14 to 1.63 mm/s (see Figure 17). This indicates a redistribution of airflow intensity away from the gap core as the microclimate thickens. Overall, the results demonstrate that microclimate thickness modulates both thermal and flow fields, with the highest sensitivity observed near the textile surface. For the ventilation simulation with a 1 mm microclimate thickness, $T_b = 20$°C, $Q_{sv} = 0.5$ dm^3/min, the computation required approximately 616 s of wall-clock time, corresponding to 1.71 CPU hours.

Conclusions

In this study, pore-scale computational models for AP and thermal resistance were created using COMSOL Multiphysics 6.2 software. It was found that increasing the complexity of polyester textile structures from a one-layer to a 3D structure reduced airflow within the textile structures, resulting in an increased thermal resistance. Consequently, multilayer and 3D textile structures provided better thermal insulation properties compared with one-layer structures. The experimental

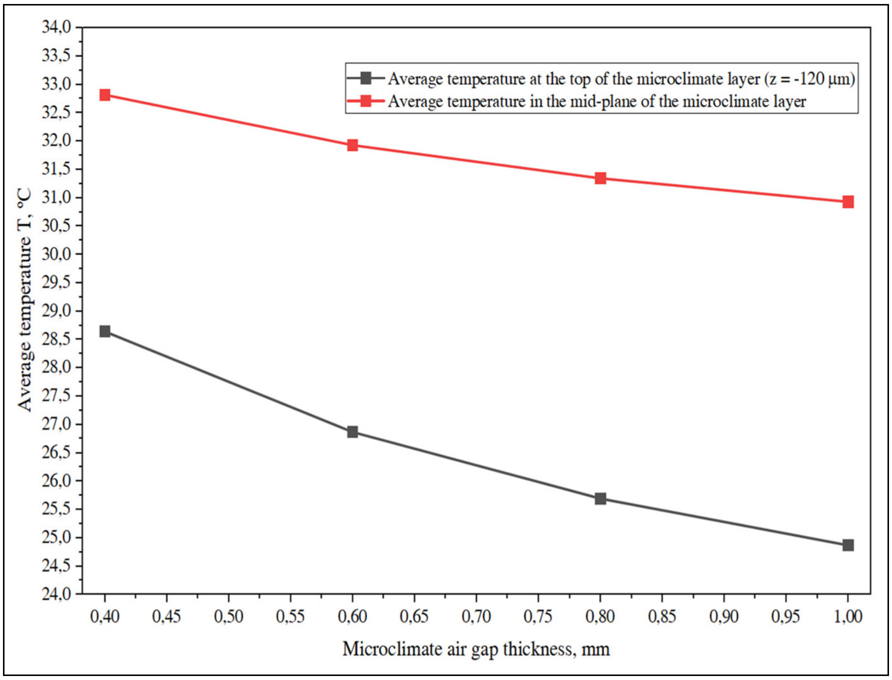

Figure 16. Influence of microclimate thickness on the average temperature at the upper boundary of the microclimate before the first textile layer and in the middle of the microclimate.

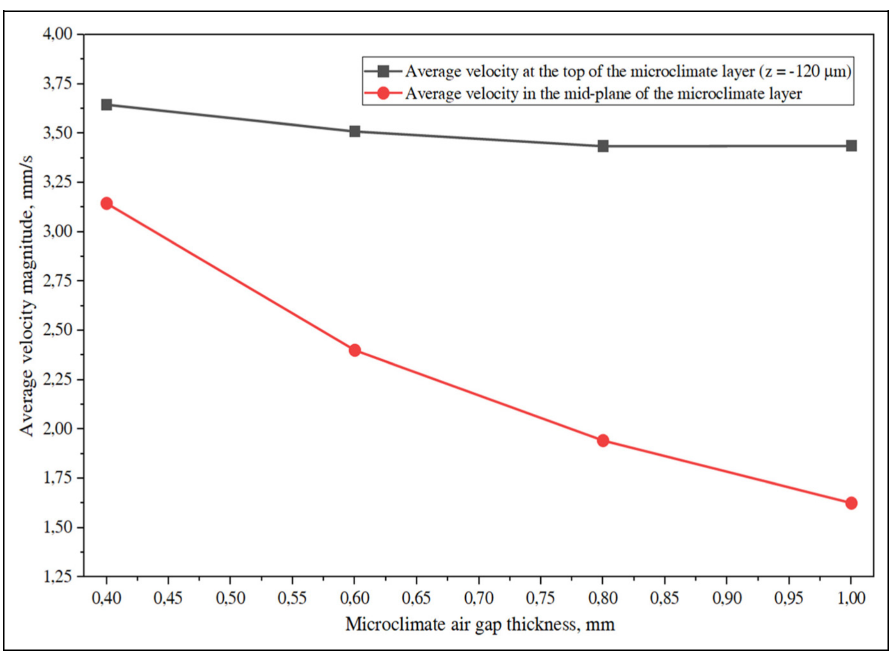

Figure 17. Influence of microclimate thickness on the average velocity magnitude at the upper boundary of the microclimate before the first textile layer and in the middle of the microclimate.

data reported in the literature and the numerical results showed good agreement.

Models with additional ventilation scenarios quantified how forced convection and supplied air temperature affect heat transfer in the microclimate. By increasing the airflow rate above 0.2 dm^3/min, the effective heat transfer coefficient increases to only a limited extent, indicating that at the higher airflow rates, the convective cooling effect gradually approaches a stable regime.

Future work will focus on extending the models to include turbulent flow regimes that may occur at higher ventilation rates. In addition, future work will include the development of a coupled heat and moisture transfer model that incorporates water-vapor transport and resistance in protective clothing systems.

Declaration of conflicting interests

The authors declared no potential conflicts of interest with respect to the research, authorship, and/or publication of this article.

Funding

The authors disclosed receipt of the following financial support for the research, authorship, and/or publication of this article: This research was funded by the Lithuanian Research Council and the Ministry of Education, Science, and Sports of the Republic of Lithuania (Project No. S-A-UEI-23-9).

ORCID iDs

Aušra Gadeikytė https://orcid.org/0000-0001-9370-4418
Rimantas Barauskas https://orcid.org/0000-0003-2147-3029

References

1. Su Y, Fan Y, Liu G, et al. A review on sustainable method to evaluate heat and moisture transfer in clothing material. *Sustain (Switz)* 2023; 15(3): 2747. DOI: 10.3390/su15032747.
2. Su Y, Tian M, Li J, et al. Development of heat and moisture transfer model for predicting skin burn of firefighter in fire environments. *J Text Inst* 2021; 113: 1658–1665.
3. Gholamreza F, Su Y, Li R, et al. Modeling and prediction of thermophysiological comfort properties of a single layer fabric system using single sector sweating torso. *Mater* 2022; 15(16): 5786. DOI: 10.3390/ma15165786.
4. Renard M and Puszkarz AK. Modeling of heat transfer through firefighters multilayer protective clothing using the computational fluid dynamics assisted by X-ray microtomography and thermography. *Mater* 2022; 15(15): 5417. DOI: 10.3390/ma 15155417.
5. Choudhary Bhoopendra U. A coupled CFD-thermoregulation model for air ventilation clothing. *Energy Build* 2022; 268: 112206. DOI: 10.1016/j.enbuild.2022.112206.
6. Tu L, Shen H and Wang F. The effective thermal resistance of permeable textile ensemble in windy environment. *Int J Therm Sci* 2021; 159: 106644. DOI: 10.1016/j.ijthermalsci.2020.106644.
7. ISO 11092:2014(EN). Textiles — Physiological effects — Measurement of thermal and water-vapour resistance under steady-state conditions (sweating guarded-hotplate test). https://www.iso.org/standard/65962.html (2014, accessed 7 September 2025).
8. Ullah HMK, Lejeune J, Cayla A, et al. A review of noteworthy/major innovations in wearable clothing for thermal and moisture management from material to fabric structure. *Text Res J* 2022; 92: 3351–3386.
9. Tessier D. *Testing thermal properties of textiles*. Duxford, England: Elsevier Ltd. DOI: 10.1016/B978-0-08-100453-1.00005-2.
10. Maduna L and Patnaik A. Heat, moisture and air transport through clothing textiles. *Text Prog* 2020; 52: 129–166.
11. ISO 9237:1995(en). Textiles — Determination of the permeability of fabrics to air. https://www.iso.org/obp/ui/en/#iso:std:iso:9237:ed-1:v1:en (accessed 20 December 2025).
12. Mishra R, Militky J and Venkataraman M. Nanoporous materials. In: *Nanotechnology in Textiles*. Cambridge, UK: Elsevier, pp. 311–353.
13. Shen H, Guo W, Wang J, et al. Investigating heat generation and transfer in hygroscopic and exothermic textiles by 3D numerical model. *Int Commun Heat Mass Transf* 2025; 165: 109053. DOI: 10.1016/j.icheatmasstransfer.2025.109053.
14. Wang H, Li J, Liu Z, et al. Three-dimensional simulation of heat and moisture transfer in woven fabric structures. *Text Res J* 2024; 94: 2232–2252.
15. Ali H, Farooq S, Siddiqui MOR, et al. Prediction of functional characteristics of interlock and rib knitted fabrics by the use of 3D computational modelling and analysis. *Hem Ind* 2025; 79: 157–168.
16. Miśkiewicz P and Cichocka A. Numerical modeling of the heat flow component of the composite developed on the basis of basalt fabric. *Autex Res J* 2024; 24(1): 20230030. DOI: 10.1515/aut-2023-0030.
17. Ismail N, Ghaddar N and Ghali K. Electric circuit analogy of heat losses of clothed walking human body in windy environment. *Int J Therm Sci* 2018; 127: 105–116.
18. Ghaddar N, Ghali K and Chehaitly S. Assessing thermal comfort of active people in transitional spaces in presence of air movement. *Energy Build* 2011; 43: 2832–2842.
19. Tu L, Qu X, Heng C, et al. Numerical analysis of heat and flow transfer in permeable textile ensemble in windy conditions. *Int J Therm Sci* 2025; 217: 110105. DOI: 10.1016/j.ijthermalsci.2025.110105.
20. Barauskas R, Valasevičiūtė L and Jurevičiūtė A. Computational analysis and experimental investigation of heat and moisture transfer in multilayer textile package. *Mat Sci (Medžiagotyra)* 2009; 15(1): 80–85.
21. Sun Y and Jasper WJ. Numerical modeling of heat and moisture transfer in a wearable convective cooling system for human comfort. *Build Environ* 2015; 93: 50–62.
22. You B, Yang J, Liu J, et al. Study of the influence of different clothing materials for mine ventilation clothing on human body and microclimate under clothing. *Sustain (Switz)* 2022; 14(20): 13460. DOI: 10.3390/su142013460.
23. Yichen D, Zheng D, Guo K, et al. Modeling heat and moisture transfer in cylindrical porous media fabrics: influencing factors and structural optimization. *Text Res J* 2025; 95(17-18): 2152–2164. DOI: 10.1177/00405175241293348.
24. Radostina AA, Kyosov M and Stankov P. Computational modelling of the heat transfer through two-layer woven structure ensembles. *Ind Text* 2020; 71: 393–397.

25. Codau E, Codau T-C, Lupu I-G, et al. Heat transfer simulation through textile porous media. *J Text Inst* 2023; 114: 257–264.
26. Li R, Dolez PI, Lai A, et al. Heat transfer through wavy clothing layers with varied permeability. *Build Environ* 2025; 280: 113114. DOI: 10.1016/j.buildenv.2025.113114.
27. Zupin Ž, Hladnik A and Dimitrovski K. Prediction of one-layer woven fabrics air permeability using porosity parameters. *Text Res J* 2011; 82: 117–128.
28. Pezzin A. *Thermo-physiological comfort modelling of fabrics and garments*. PhD thesis. Polytechnic University of Turin, Italy 2015. DOI: 10.6092/polito/porto/2591973.
29. Dejene BK and Gudayu AD. Exploring the potential of 3D woven and knitted spacer fabrics in technical textiles: A critical review. *J Ind Text* 2024; 54: 1–55. DOI: 10.1177/15280837241253614.
30. Zienkiewicz OC, Taylor RL and Nithiarasu P. *The finite element method for fluid dynamics*. 6th ed. Amsterdam: Elsevier, 2005.
31. Vafai K. *Handbook of porous media*. 2nd ed. Boca Raton: Taylor & Francis Group, LLC, 2005.
32. Elgeti S and Sauerland H. Deforming fluid domains within the finite element method: Five mesh-based tracking methods in comparison. *Arch Comput Methods Eng* 2016; 23: 323–361.
33. Xiao X, Zeng X, Long A, et al. An analytical model for through-thickness permeability of woven fabric. *Text Res J* 2012; 82: 492–501.
34. Gebart BR. Permeability of unidirectional reinforcements for RTM. *J Compos Mater* 1992; 26: 1100–1133.
35. Carman PC. *Flow of gases through porous media*. London: Butterworths Scientific Publications. 1956. DOI: 10.1038/178824a0.
36. Alotaibi H, Jabbari M and Soutis C. A numerical analysis of resin flow in woven fabrics: Effect of local tow curvature on dual-scale permeability. *Mater* 2021; 14: 405.
37. Geoffre A, Wielhorski Y, Moulin N, et al. Influence of intra-yarn flows on whole 3D woven fabric numerical permeability: From Stokes to Stokes–Darcy simulations. *Int J Multiphase Flow* 2020; 129: 103349. DOI: 10.1016/j.ijmultiphaseflow.2020.103349.
38. Siddiqui MOR, Farooq S, Husain MD, et al. Prediction of air permeability and effective thermal conductivity of multifilament polyester yarn by finite element analysis. *Polimery/Polymers* 2023; 68: 6–18.
39. COMSOL. *COMSOL Multiphysics Reference Manual*. https://doc.comsol.com/6.4/docserver/#!/com.comsol.help.comsol/comsol_ref_mesh.24.24.html%23576386 (2025, accessed 21 December 2025).
40. Yang T, Xiong X, Petrů M, et al. Theoretical and experimental studies on thermal properties of polyester nonwoven fibrous material. *Mater* 2020; 13(12): 2882. DOI: 10.3390/ma13122882.
41. Siddiqui MOR and Sun D. Finite element analysis of thermal conductivity and thermal resistance behaviour of woven fabric. *Comput Mater Sci* 2013; 75: 45–51.
42. Morton WE and Hearle JWS. *Physical properties of textile fibres*. 4th ed. Cambridge: Woodhead Publishing Limited and CRC Press LLC, 2008.
43. Militký J and Křemenáková D. A simple methods for prediction of textile fabrics thermal conductivity. In: Meyer, Josua P (ed.), *5th International conference on heat transfer, fluid mechanics and thermodynamics*. South Africa: Sun City, 1–4 July, 2007, pp. 1–5.
44. Siddiqui MOR and Sun D. Thermal analysis of conventional and performance plain woven fabrics by finite element method. *J Ind Text* 2018; 48: 685–712.
45. Siddiqui MOR and Sun D. Computational analysis of effective thermal conductivity of microencapsulated phase change material coated composite fabrics. *J Compos Mater* 2015; 49: 2337–2348.
46. Zhang Y, Jia J and Guo Z. Numerical investigation of heat transfer in a garment convective cooling system. *Fash Text* 2022; 9: 2. DOI: 10.1186/s40691-021-00276-3.
47. Barauskas R and Abraitiene A. A model for numerical simulation of heat and water vapor exchange in multilayer textile packages with three-dimensional spacer fabric ventilation layer. *Text Res J* 2011; 81: 1195–1215.
48. Gadeikytė A, Abraitienė A and Barauskas R. Application of combined micro- and macro-scale models to investigate heat and mass transfer through textile structures with additional ventilation. *Math* 2023; 11(11): 2532. DOI: 10.3390/math11112532.
49. Libreros J and Trujillo M. Effects of mesh generation on modelling aluminium anode baking furnaces. *Fluids* 2021; 6(4): 140. DOI: 10.3390/fluids6040140.
50. Martinez JM. Algorithms for solving nonlinear systems of Equations. In: Spedicato E (ed.). *Algorithms for continuous optimization NATO ASI series (Series C: Mathematical and physical sciences)*. Springer: Dordrecht, Netherlands, Vol. 434. 1994, pp.81–108.
51. Schenk O, Gärtner K and Fichtner W. Scalable parallel sparse factorization with left-right looking strategy on shared memory multiprocessors. In: Sloot P, Bubak M, Hoekstra A, Hertzberger B. (eds). *Lecture notes in computer science (including subseries lecture notes in artificial intelligence and lecture notes in bioinformatics)*. Springer: Berlin, Heidelberg, Vol. 1593. 1999, pp.221–230.
52. Siddiqui MOR and Sun D. Automated model generation of knitted fabric for thermal conductivity prediction using finite element analysis and its applications in composites. *J Ind Text* 2016; 45: 1038–1061.
53. Zemzem M, Hallé S and Vinches L. Thermal insulation of protective clothing materials in extreme cold conditions. *Saf Health Work* 2023; 14: 107–117.
54. Sabantina L and Ehrmann A. New testing device for air permeability. *Commun Dev Assem Text Prod* 2023; 4: 164–170.
55. Torres EG, Psikuta A and DenHartog E. Impact of garment construction and environmental factors on heat transfer. *Int J Biometeorol* 2025; 69: 1495–1504.
56. Sargolzaei G, Mousazadegan F, Ezazshahabi N, et al. Investigation of microclimate ventilation of simulated garment in terms of wind speed and air gap thickness. *Fibers Polym* 2021; 22: 2063–2069.